JOURNAL OF PROPULSION AND POWER
Vol. 24, No. 2, March–April 2008

Testing of a 250-Kilowatt Fault-Tolerant Permanent Magnet Power Generation System for Aeroengines

Z. Sun,* J. D. Ede,† J. Wang,‡ and G. W. Jewell§
University of Sheffield, Sheffield, England S1 3JD, United Kingdom
and
J. J. A. Cullen¶ and A. J. Mitcham**
Rolls–Royce plc, Derby, England DE24 8BJ, United Kingdom

DOI: 10.2514/1.32158

This paper describes the experimental testing of a 250-kW fault-tolerant permanent magnet power generation system (machine and converter) for the low-pressure shaft of a large civil engine. The relative merits of this system as a reliable electrical power source for safety critical applications are discussed, and its performances under both healthy and fault conditions are analyzed and experimentally tested. It has been shown that the power generation system has a high efficiency over a wide output power range under healthy conditions. However, a large torque ripple and potentially destabilizing shaft power swing will result under an open- or short-circuit fault condition. This problem can be eliminated by employing an optimal torque control strategy. The utility and effectiveness of the control technique have been experimentally validated.

I. Introduction

THE more-electric aircraft (MEA) promises significantly more efficient and reliable power generation, distribution, and utilization over their more conventional counterparts [1]. However, the increased use of electrical power imposes very onerous demands on the electrical power system, in terms of the level of electrical power to be generated and issues related to the reliability, power quality, and stability [2]. Embedded generators which are mounted coaxially with the main shafts eliminate the need for takeoff shafts and associated gearboxes and therefore offer potential for simplicity, increased capacity, and reliability. Of various embedded electrical generator technologies, switched reluctance (SR) generators are often regarded as having great potential because of their inherent fault tolerance and their ability to operate in harsh environments [3–5]. However, their power density is often compromised by the need to incorporate a large working air gap to accommodate thermal expansion and mechanical clearance specifications over the wide range of operating conditions encountered in service. A fault-tolerant permanent magnet (PM) generator, on the other hand, can more readily tolerate a large air gap with minimal reduction in performance, while also offering a high power density and efficiency. It is therefore emerging as a competitive generator technology for MEA power systems.

A key requirement for many aircraft generation systems is a degree of fault tolerance, that is, an ability to continue operating at or near rated power in the event of a single point fault in the generator or its associated converter. The PM machine described in this paper employs a number of design features to enhance its fault-tolerant capability [6,7]. The phase windings are physically, magnetically, and electrically isolated, as shown schematically in Fig. 1 for one quarter of a five-phase fault-tolerant PM machine. Consequently, a fault in one phase will not readily propagate to the adjacent phases. In addition, each phase winding is designed to have one per-unit self-reactance in order to limit short-circuit current at fault conditions to its rated value. Further, by employing a multiphase (usually >4) design, the machine can continue to provide a useful power output even with a fault in one of the phases. These design features, when combined with the high power density of PM machines, make a fault-tolerant PM machine an attractive option in a safety critical application.

Generally, it is assumed that such fault-tolerant machines have a sinusoidal back-emf waveform, so that the current controller is required to track a set of sinusoidal current commands proportional to a given torque demand [8–10]. However, this simple control strategy inevitably results in an undesirable torque ripple during normal operation if the back-emf waveform is nonsinusoidal and a large torque pulsation under a fault condition, such as an open-circuited or a short-circuited phase. Although this problem may be partly overcome by adopting an optimal torque control strategy which is aimed at minimizing the copper loss when delivering the required torque demand [11–13], the effectiveness of such a strategy is limited by the available converter voltage, because, by minimizing the copper loss, the resulting current command tends to be increasingly in phase with the back-emf. Consequently, at high speed the controller cannot track the commanded currents due to the limited converter voltage. A generalized optimal torque control strategy for fault-tolerant permanent magnet brushless drives has been reported in [14] and demonstrated in [15]. It has been shown that a ripple-free torque can be produced under both healthy and faulted conditions in both the constant torque and constant power operating regions. However, the realization of such control strategies for fault-tolerant PM brushless machines is entirely reliant on an effective fault detection technique.

Although the use of a fault-tolerant PM machine as a reliable and power-dense actuator for safety critical applications has been extensively reported, its potential as a high capacity power generator for MEA power systems has not been comprehensively studied and demonstrated. This paper reports the experimental testing of a 250-kW fault-tolerant PM generation system operating under both

Presented as Paper 4829 at the 5th International Energy Conversion Engineering Conference and Exhibit, St. Louis, MO, 25–27 June 2007; received 15 May 2007; revision received 3 December 2007; accepted for publication 5 December 2007.

*Ph.D. Student, Department of Electrical and Electronic Engineering; Z.Sun@shef.ac.uk.
†Research Associate, Department of Electrical and Electronic Engineering; J.D.Ede@shef.ac.uk.
‡Reader, Department of Electrical and Electronic Engineering; J.B.Wang@shef.ac.uk.
§Professor, Department of Electrical and Electronic Engineering; G.Jewell@shef.ac.uk.
¶Electrical Machines Specialist, Strategic Research Centre, PO Box 31.
**Consultant, Strategic Research Centre, PO Box 31.

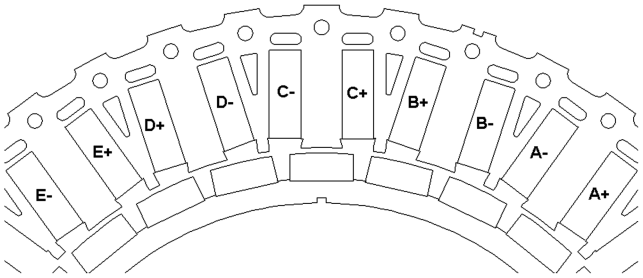

Fig. 1 Schematic of one quarter of a 250-kW, five-phase fault-tolerant PM generator.

healthy and fault conditions for the low-pressure shaft of a large civil engine. It has been shown that, by employing an optimal torque control strategy, large electromagnetic torque ripple and shaft power fluctuations caused by a fault condition can be considerably reduced. This demonstrates that the system can maintain a smooth mechanical input power under both a single phase open- and short-circuit condition.

II. 250-kW Fault-Tolerant PM Generation System and its Testing Rig

A five-phase, fault-tolerant PM generator [16] with sinusoidal back-emf and capable of 250-kW rated output power has been designed and manufactured. This generator was designed with all the fault-tolerance features described in the previous section and therefore has the capability to operate continuously even with one phase winding open- or short-circuited. Under an open- or short-circuit condition, the generator can still provide 80% of the rated power with the remaining four healthy phases in operation. The cross section of one quarter of the generator is shown in Fig. 1 and its specifications are summarized in Table 1.

To measure the characteristics of the fault-tolerant generator and to test the performance of the power generation system, an experimental testing rig has been established. Figure 2 shows the schematic of the testing rig for the fault-tolerant power generation system. The generator is coupled via a Lebow TMS 9000 series in-line torque transducer to the shaft of a 350-kW dynamometer which provides the mechanical input power at a given regulated speed. Five separate H-bridge converters are employed to control the generator phase currents and hence to regulate its output power over a wide speed range, Fig. 3. Each H-bridge converter consists of four 600-A/1200-V insulated gate bipolar transistor (IGBT) devices and is controlled by a dSPACE hardware-in-the-loop system via an analog-to-digital interface and a unipolar pulse width modulator (PWM) operating at 7.0-kHz switching frequency. The output power of the generator is fed to the three phase 415-V mains via a 350-V 4-quadrant dc sink/source.

The control of the power generation system is achieved by two feedback loops. An outer torque control loop, which implements an optimal torque control strategy as will be briefly outlined in the subsequent section, controls the generator torque/power and power flow, and outputs a current reference for each phase. These current references are tracked by five independent current controllers using feedback from the current transducer (CT) in each phase. The resulting voltage control signal for each phase is fed to a PWM modulator which controls the switching states of the H bridge via optic fiber links. The PWM modulator also monitors the operating conditions of the H bridge, and provides appropriate trip and reset

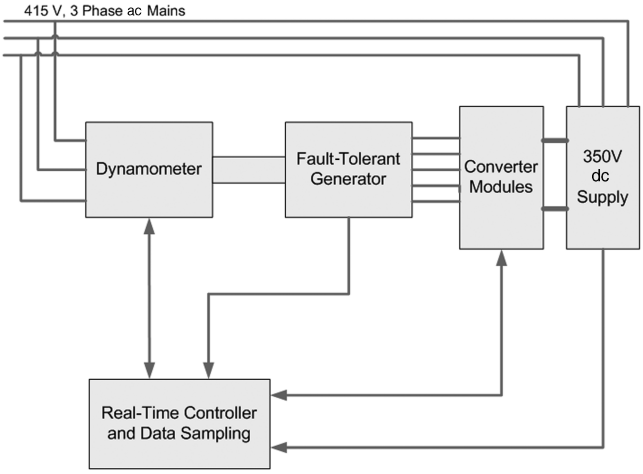

Fig. 2 Schematic of testing rig for fault-tolerant PM generation system.

signals also via optic links for various protections, such as under voltage, over current, and over heating. Both the torque and current control algorithms are implemented in real time in the dSPACE system.

Various tests have been carried out to characterize the performance of the power generation system under healthy conditions. By way of example, Fig. 4a compares the measured and finite element (FE) predicted phase back-emf at a speed of 200 rpm. A similar comparison for short-circuit currents which results when all five phases are short-circuited is given in Fig. 4b. As will be seen, the phase back-emf is essentially sinusoidal with total harmonic distortion, which is dominant by third, fifth, and seventh harmonics, being less than 5%. However, for a five-phase machine, only 9th, 11th, 19th, 21st, ..., harmonics interact with a sinusoidal phase current to produce a torque ripple [17]. Because the machine is designed to have one per-unit phase inductance, both the measured and predicted steady-state peak short-circuit currents are close to the rated peak current of 464 A. However, the measured short-circuit current is slightly less than the predicted value, due to the fact that the leakage inductance of the end winding and parasitic inductance of the connection cable are not accounted for in the FE prediction. A short-circuit test of a single phase was also undertaken (the remaining phases being open-circuited), and the resulting short-circuit current waveform is virtually the same as that observed in the balanced short-circuit condition because the mutual inductance between phases is very small ($<3\%$).

Figure 5 shows the variation of the generator average torque with peak phase current under healthy conditions when the current in each phase is maintained sinusoidally in phase with its back-emf by closed-loop current control. As will be seen, a linear torque-current characteristic is observed.

The efficiency of the power generation system under various load conditions has been evaluated by measuring the average input mechanical power (product of the torque and speed) and the average electrical output power (product of dc-link voltage and current) to the dc sink. The resulting inferred efficiency at 1050 rpm as a function of the input mechanical power is plotted in Fig. 6. It is evident that an overall system efficiency greater than 90% is achieved over a wide power range and this result is consistent with the predicted average generator efficiency of 95.5% and the average power electronic converter efficiency of 94.5%.

Table 1 Specification of five-phase fault-tolerant PM generator

Rated speed	1050 rpm	Phase inductance	307 μH
Rated torque	2274 N · m	Phase resistance	0.56 mΩ
Rated power	250 kW	Rated phase current (peak)	464 A
dc-link voltage	350 V	Number of pole pair	14
Back-emf (peak)	218 V at 1050 rpm	Number of slots	40

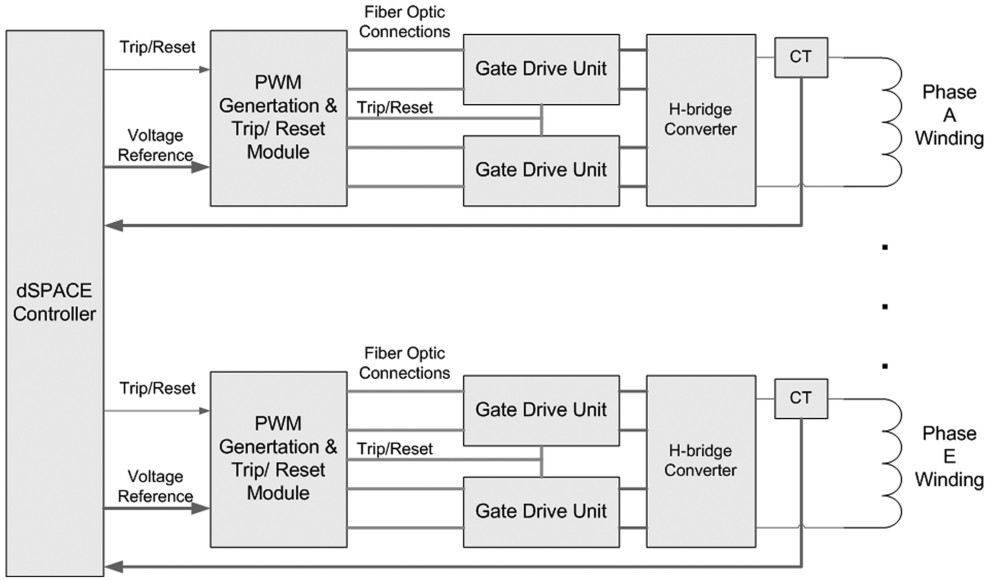

Fig. 3 Control system schematic for fault-tolerant PM generation system.

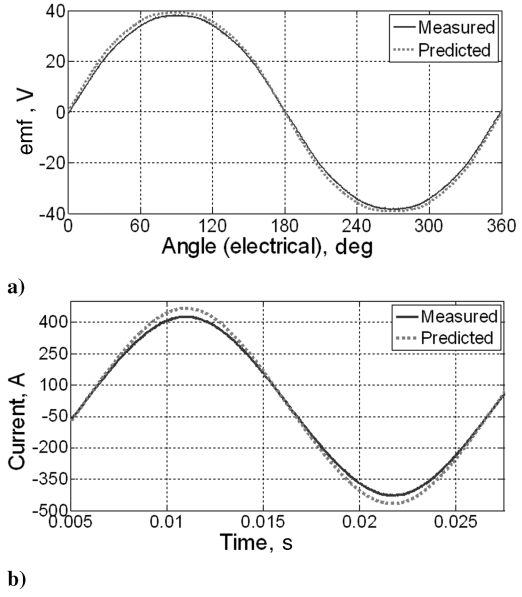

Fig. 4 Comparison of measured and predicted back-emfs and short-circuit currents. a) Back-emf; b) short-circuit current at 200 rpm.

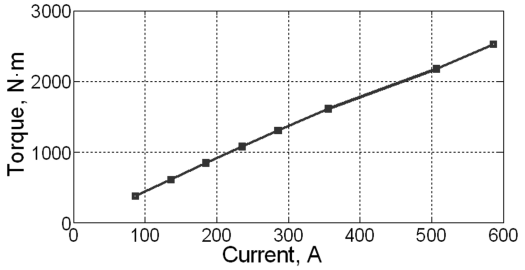

Fig. 5 Measured variation of torque with peak phase current.

III. Performance Under Fault Conditions

The fault-tolerant PM generator is designed to operate continuously under fault conditions such as a single phase open- or short-circuit. To eliminate a large torque ripple and potentially destabilizing shaft power swing under these conditions, an optimal torque control strategy [14] is employed and is briefly outlined.

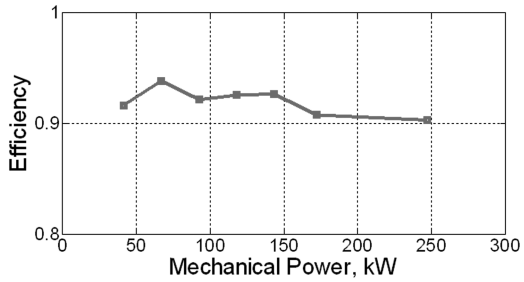

Fig. 6 Measured variation of system efficiency with input power.

For an m-phase permanent magnet machine equipped with a surface-mounted magnet rotor, the electromagnetic torque T_e, which results when a fault occurs on phase k, is given by

$$T_e = \sum_{j\neq k}^{m} a_j(\theta) i_j + \begin{cases} 0 & \text{for an open-circuit fault} \\ a_k(\theta) i_k & \text{for a short-circuit fault} \end{cases} \quad (1)$$

where i_j is the instantaneous current in phase j, and $a_j(\theta) i_j = p(\mathrm{d}\psi_j/\mathrm{d}\theta) i_j$ is the instantaneous torque of phase j at a given rotor angular position θ, where ψ_j is the magnet flux linkage with phase j and p is the number of pole pairs, and similarly for the faulted phase k. For a given torque demand T_d, the optimal instantaneous currents in the healthy phases can be determined by minimizing the copper loss p_{cu}:

$$p_{\mathrm{cu}} = R \sum_{j\neq k}^{m} i_j^2 \quad (2)$$

subject to the following constraint:

$$T_d = \sum_{j\neq k}^{m} a_j(\theta) i_j + T_r \quad (3)$$

where R is the phase resistance of the machine, and T_r is given by

$$T_r = \begin{cases} 0 & \text{for an open-circuit fault} \\ a_k(\theta) i_k & \text{for a short-circuit fault} \end{cases} + T_{\mathrm{cg}}(\theta) \quad (4)$$

represents the uncontrollable torque ripple caused by a winding fault and the cogging torque $T_{\mathrm{cg}}(\theta)$, which may still exist even if all of the design parameters have been optimized. A closed form solution for the above optimization may be obtained using the quadratic

programming technique, and the resulting instantaneous phase currents are given by

$$i_j = a_j(\theta)(T_d - T_r) \Big/ \sum_{j \neq k}^{m} [a_j(\theta)]^2 \tag{5}$$

Because the speed of the generator is essentially dictated by the prime mover, a smoothly controllable torque implies the generator power can be regulated at any desired level according to demand.

A. Single Phase Open-Circuit Fault

The behavior of the fault-tolerant generation system under an open-circuit fault was tested first because the resulting torque ripple is relatively small compared with that which results from a short-circuit fault [16]. The test was carried out with phase E being open-circuited when the generator was operating at the rated speed of 1050 rpm, and the optimal torque control strategy given by Eq. (5) for generating the current references in the remaining healthy phases was realized in real time. Figure 7a compares the measured and predicted torque waveforms under the open-circuit conditions with and without the optimal torque control (OTC) being implemented.

It is apparent that the measured and predicted average torques under the open-circuit condition without optimal torque control are lower than both the desired value of 1500 N · m and the measured and predicted averages which result with the optimal torque control. This is because, without optimal torque control, the torque reduction due to one phase being out of service is not compensated for. However, the frequency and magnitude of the predicted torque ripple which results without optimal torque control are much greater than the measured values. Further, the measured torque ripple which results when the optimal torque control has been implemented is also much greater than the prediction. These discrepancies are likely due to the combined effects of the mechanical characteristic of the testing rig and the dynamic behavior of the dynamometers because the measured torque is not purely the electromagnetic torque produced by the generator but the combined torque output which contains the torque generated by the dynamometer as well as the effect of the system inertia. Thus, on one hand, the inertia of the testing rig and the actively controlled dynamometer act as a low pass filter which attenuates high frequency torque ripples resulting from the open-circuit fault. On the other hand, the dynamometer itself generates torque ripple with its own characteristic frequency, as illustrated in Fig. 7b where the generator is not loaded and the torque ripple results predominately from the dynamometer. Clearly, this torque ripple will neither be reduced by the optimal torque control, nor be attenuated by the dynamometer itself. Consequently, the measured torque ripple under the optimal torque control is the combined effect of the low pass filter and the characteristic torque ripple of the dynamometer, as will be evident when comparing the measured torque waveform in Fig. 7a under optimal torque control with that in Fig. 7b under no load.

The foregoing analysis indicates that due to the limitation of the testing rig, direct torque measurement will not provide a convincing demonstration of the effectiveness of the optimal torque. To circumvent this problem, the electromagnetic torque of the generator is, instead, calculated using the measured phase currents, i_j and back-emfs, e_j ($j = A, B, C, \ldots,$) and the generator speed ω according to the following power balance equation:

$$T = \frac{1}{\omega}\left(\sum_{j=A,B,\ldots} e_j i_j \right) \tag{6}$$

The torque obtained using Eq. (6) is denoted as indirectly measured torque. The predicted and indirectly measured torque waveforms under the open-circuit fault condition without optimal torque control are now compared in Fig. 8. It is evident that the prediction agrees well with the indirectly measured values.

As can be seen in Fig. 8, a large peak-to-peak torque variation up to ~500 N · m or 22% of the rated torque results under the open-circuit fault condition. It can be inferred that if sinusoidal currents in the remaining healthy phases are maintained, a similar shaft power swing of more than 22% would result because the speed of the prime mover, that is, the low pressure (LP) shaft, is more or less constant. If this problem is not effectively dealt with, the performance of the power generation system under fault conditions could be problematic because the torque ripple may excite undesirable vibration modes within the mechanical system while the large swing in the electrical output power would lead to unacceptable power quality, and may even affect network stability. This problem can, however, be avoided by employing the optimal torque control strategy. Figure 9 compares the measured and simulated phase current waveforms at 1050 rpm which result with the optimal torque control strategy when phase E is open-circuited and the remaining phases are producing a total output power of 165 kW. As will be seen, to compensate for the torque ripple produced by the faulted phase, the current waveforms in the remaining healthy phases are no longer sinusoidal. Figure 10 compares the indirectly measured and predicted torque waveforms when the optimal torque control is applied. It is evident that with the optimal torque control the torque ripple due to the open-circuit fault is virtually removed, and consequently the power generation system outputs smooth power to the dc network.

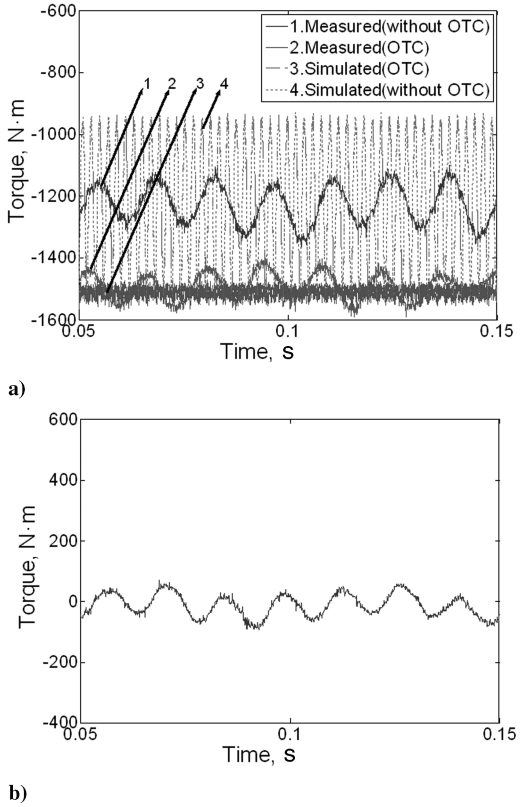

Fig. 7 Measured and predicted torque waveforms. a) Comparison of measured and predicted torque waveforms; b) torque ripple generated by dynamometer on no load.

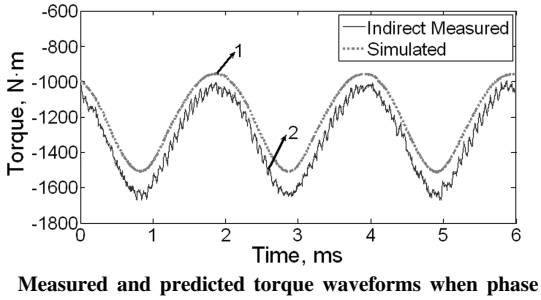

Fig. 8 Measured and predicted torque waveforms when phase E is open-circuited at 1050 rpm.

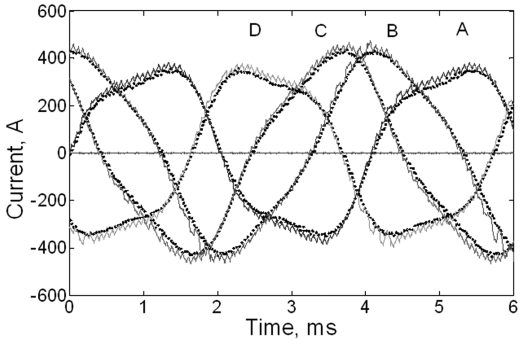

Fig. 9 Measured (solid line) and predicted (dotted line) current waveforms with optimal torque control when phase *E* is open-circuited at 1050 rpm.

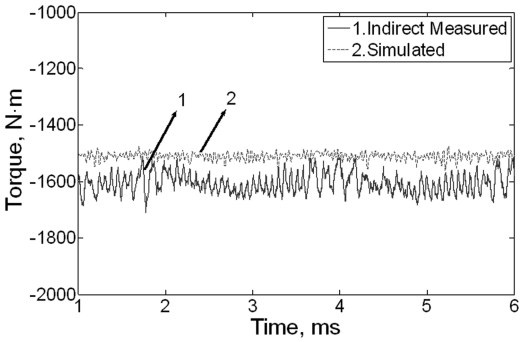

Fig. 10 Measure and predicated torque waveforms with optimal torque control when phase *E* is open-circuited at 1050 rpm.

B. Single Phase Short-Circuit Fault

As indicated in the previous section, a steady-state short-circuit current in any phase is effectively limited to the rated value, and hence the generator can sustain terminal short-circuit faults indefinitely without overheating. However, a larger torque ripple will be produced due to the interaction of the short-circuit current with the field of the rotor permanent magnets. Figure 11 shows the measured and predicted torque waveforms resulting from a single phase short circuit at 100 rpm with the remaining phases on open circuit. Because the frequency of the torque ripple is much lower than that under the open-circuit fault condition of Fig. 7, the ripple attenuation due to the low pass filter effect of the testing rig is insignificant, and hence the measured and predicated torque ripples are in reasonably good agreement. As can be seen, a peak-to-peak torque variation of $\sim$1000 N $\cdot$ m or 44% of the rated torque results under the short-circuit condition. If this torque ripple is not corrected, a similar level of shaft power swing would occur, which would be detrimental to the mechanical system performance and stability.

However, this torque ripple can be eliminated by shaping the currents in the healthy phases according to the optimal torque control strategy given by Eq. (5) while still producing the required 80% of output power. Figure 12 compares the measured and simulated phase current waveforms which result with the optimal torque control

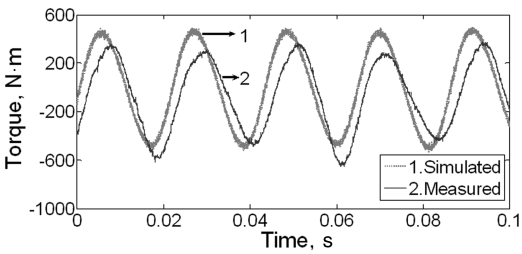

Fig. 11 Comparison of measured and predicted torque ripples with single phase short-circuit fault.

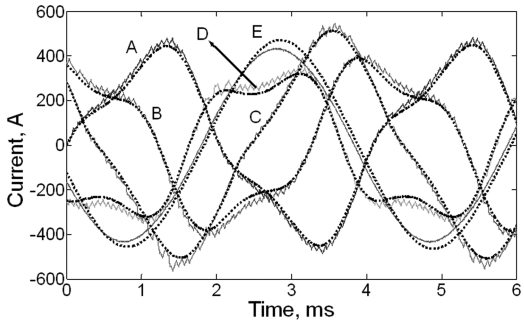

Fig. 12 Measured (solid line) and predicted (dotted line) current waveforms with optimal torque control when phase *E* is short-circuited.

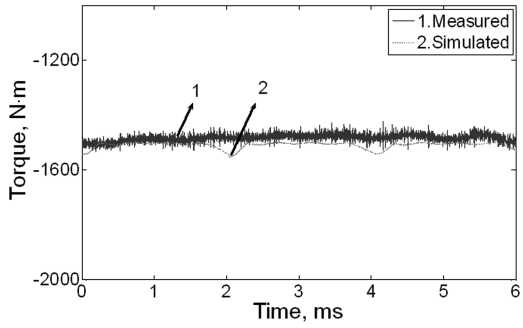

Fig. 13 Measure and predicated torque waveforms with optimal torque control when phase *E* is short-circuited.

strategy when phase *E* is short-circuited. The resulting torque waveform is shown in Fig. 13 where it can clearly be seen that the large torque ripple caused by phase *E* short-circuit current has now been removed. It should be noted that the torque ripple resulting from the dynamometer still exists, although it is not obvious in Fig. 13 due to the short time scale in the plot.

IV. Conclusions

The merits and potentials of a 250-kW fault-tolerant permanent magnet generation system for aerospace applications have been analyzed and experimentally demonstrated, and its performance under both healthy and fault conditions characterized. It has been shown that the system efficiency under healthy operating conditions is greater than 90% over a wide output power range. It has also been shown that although the short-circuit current is limited to the rated value, a short-circuit fault will cause a large torque ripple and destabilizing shaft power swing. This problem can be eliminated by employing an optimal torque control strategy. The utility and effectiveness of the control technique have been experimentally validated.

Acknowledgments

The authors would like to thank Rolls–Royce plc and the U.K. Government Department of Trade and Industry for jointly funding this project, and the U.K. Engineering and Physical Sciences Research Council for their financial support in establishing the dynamometer facility.

References

[1] Quigley, R. E., Jr., "More Electric Aircraft," *Proceedings of the of 1993 IEEE Applied Power Electronics Conference*, IEEE, Piscataway, NJ, 1993, pp. 906–911.

[2] Weimer, J. A., "Electrical Power Technology for the More Electric Aircraft," *Proceedings of the of IEEE 12th Digital Avionics Systems Conference*, IEEE, Piscataway, NJ, 1993, pp. 445–450.

[3] Radun, A. V., "High-Power Density Switched Reluctance Motor Drive for Aerospace Applications," *IEEE Transactions on Industry*

Applications, Vol. 28, No. 1, 1992, pp. 113–119. doi:10.1109/28.120219

[4] Ferreira, C. A., Jones, S. R., Heglund, W. S., and Jones, W. D., "Detailed Design of a 30 kW Switched Reluctance Starter/Generator System for a Gas Turbine Engine Application," *IEEE Transactions on Industry Applications*, Vol. 31, No. 3, 1995, pp. 553–561. doi:10.1109/28.382116

[5] Husain, I., Radun, A., and Nairus, J., "Fault Analysis and Excitation Requirements for Switched Reluctance Generators," *IEEE Transactions on Energy Conversion*, Vol. 17, No. 1, 2002, pp. 67–72. doi:10.1109/60.986439

[6] Jack, A. G., Mecrow, B. C., and Haylock, J. A., "A Comparative Study of Permanent Magnet and Switched Reluctance Motors for High-Performance Fault-Tolerant Operation," *IEEE Transactions on Industry Applications*, Vol. 32, No. 4, 1996, pp. 889–895. doi:10.1109/28.511646

[7] Mecrow, B. C., Jack, A. G., Haylock, J. A., and Coles, J., "Fault-Tolerant Permanent Magnet Machine Drives," *IEE Proceedings–Electric Power Applications*, Vol. 143, No. 6, 1996, pp. 437–442. doi:10.1049/ip-epa:19960796

[8] Radaelli, M., Sozzi, L., and Ehrhart, P., "Novel Technologies with PM-Machines for Ship Propulsion," *Proceedings of All-Electric Ship Conference*, Institute of Marine Engineering, Paris, 1997, pp. 17–22.

[9] Haylock, J. A., Mecrow, B. C., Jack, A. G., and Atkinson, D. J., "Operation of Fault Tolerant Machines with Winding Failures," *IEEE Transactions on Energy Conversion*, Vol. 14, No. 4, 1999, pp. 1490–1495. doi:10.1109/60.815095

[10] Haylock, J. A., Mecrow, B. C., Jack, A. G., and Atkinson, D. J., "Online Detection of Winding-Short Circuits in Inverter Fed Drives," *9th International Conference on Electrical Machines and Drives*, IEE CP No. 468, Institution of Electrical Engineering, Canterbury, U.K., 1999, pp. 258–262.

[11] Ede, J. D., Atallah, K., Wang, J., and Howe, D., "Modular Fault-Tolerant Permanent Magnet Brushless Machines," *Proceedings of the PEMD2002*, Institution of Electrical Engineering, Bath, U.K., 2002, pp. 415–420.

[12] Hanselman, C., "Minimum Torque Ripple, Maximum Efficiency Excitation of Brushless Permanent Magnet Motors," *IEEE Transactions on Industrial Electronics*, Vol. 41, No. 3, 1994, pp. 292–300. doi:10.1109/41.293899

[13] French, C., and Acarnley, P., "Direct Torque Control of Permanent Magnet Drives," *IEEE Transactions on Industry Applications*, Vol. 32, No. 5, 1996, pp. 1080–1088. doi:10.1109/28.536869

[14] Wang, J., Atallah, K., and Howe, D., "Optimal Torque Control of Fault-Tolerant Permanent Magnet Brushless Machines," *IEEE Transactions on Magnetics*, Vol. 39, No. 5, 2003, pp. 2962–2964. doi:10.1109/TMAG.2003.816707

[15] Max, L., Wang, J., Atallah, K., and Howe, D., "Real-Time Optimal Torque Control of Fault-Tolerant Permanent Magnet Brushless Machines," *Journal of Applied Physics*, Vol. 97, No. 10, 2005, pp. 10N510-1–10N510-3. doi:10.1063/1.1852439

[16] Ede, J. D., Jewell, G. W., Atallah, K., and Powell, D. J., "Design of a 250 kW, Fault-Tolerant PM Generator for the More-Electric Aircraft," AIAA Paper 2005-5644, 15–18 Aug. 2005.

[17] Atallah, K., Wang, J., and Howe, D., "Torque Ripple Minimisation in Modular Permanent Magnet Brushless Machines," *IEEE Transactions on Industry Applications*, Vol. 39, No. 6, 2003, pp. 1689–1695. doi:10.1109/TIA.2003.818986

A. Prasad
Associate Editor